Ng, C. W. W. *et al*. (2017) ***Géotechnique Letters* 7**, 79–89, http://dx.doi.org/10.1680/jgele.16.00159

Influence of particle size on the mechanism of dry granular run-up on a rigid barrier

C. W. W. NG*, C. E. CHOI*†, L. H. D. LIU*, Y. WANG‡, D. SONG* and N. YANG*

Granular flows comprise a wide range of particle sizes. The particle size governs the degree of grain contact and inertial stresses in the flow, thus influencing the mechanism of impact against a rigid barrier. The current commonly adopted design approaches estimating the run-up height are based on the energy principle and the momentum approach. However, both neglect the discrete nature of flows, and do not consider the effects of particle size on the flow regime. In this study, physical experiments using different sizes of monodispersed sand and glass spheres were carried out to investigate the run-up mechanisms on a rigid barrier. Results have shown that the run-up height is not only dependent on the Froude number of the flow before impact, but also on the particle size which principally governs the mechanism of run-up. Inertial flows comprising large particles (the Savage number (N_{Sav}) > 0·1) profoundly transfer momentum vertically upon impact, resulting in significant grain saltation and high run-up heights. In contrast, frictional flows comprising fine particles (N_{Sav} < 0·1) tend to pile up without significant run-up due to a high degree of contact stresses. This implies that for flows with coarse particles entrained at the front of the flow by way of particle-size segregation, the run-up height is principally influenced by large particles that accumulate at the flow front.

KEYWORDS: geophysics; landslides; model tests

NOTATION

E	modulus of elasticity of solid particles
E_f	final energy of the flow impacting the rigid barrier (J)
E_i	initial energy of the flow approaching the rigid barrier (J)
e	coefficient of restitution of solid particles
$\boldsymbol{g}$	gravitational acceleration (m/s^2)
h	characteristic flow depth (m)
h_f	run-up height (m)
L	length of the block (m)
m	mass of the flow (kg)
N_{Fr}	the Froude number
N_{Sav}	the Savage number
P	mean normal stress (Pa)
P_B	normal stress applied at the boundary of the shear region (Pa)
s	factor describing the angularity or sphericity of the solid particles
T	travel time of the flow
u	speed of an upstream propagating bore from the rigid barrier (m/s)
v	bulk flow velocity (m/s)
$\langle v^2\rangle^{1/2}$	translational velocity from particle interaction (m/s)
$\langle w^2\rangle^{1/2}$	rotational velocity from particle interaction (m/s)
$\dot{\gamma}$	shear rate (1/s)
δ	characteristic particle diameter (m)
θ	channel inclination (deg)
μ	surface coefficient of friction
ρ	bulk density of the flow (kg/m^3)
ρ_f	density of debris flow in contact with the barrier (kg/m^3)
ρ_i	density of upstream flow (kg/m^3)
ρ_P	solid density of the granular material (kg/m^3)
$\boldsymbol{\sigma}_{ij}$	mean normal stress tensor
$\boldsymbol{\tau}_{ij}$	stress tensor
$\bar{\boldsymbol{\tau}}_{ij}$	deviatoric stress (Pa)
υ	solids fraction of the flow of solid particles
ϕ	dynamic friction angle of the flow material (deg)

Manuscript received 31 October 2016; first decision 10 February 2017; accepted 11 February 2017.
Published online at www.geotechniqueletters.com on 2 March 2017.
*Department of Civil and Environmental Engineering, The Hong Kong University of Science and Technology, Kowloon, Hong Kong.
†The HKUST Jockey Club Institute for Advanced Study, Kowloon, Hong Kong.
‡Department of Architecture and Civil Engineering, City University of Hong Kong, Kowloon, Hong Kong.

INTRODUCTION

Geophysical flows comprise a wide range of particle sizes (Jakob *et al*., 2005) that vary spatially within the flow mass, by way of processes such as particle-size segregation (Gray & Chugunov, 2006; Johnson *et al*., 2012). Pouliquen (1999) demonstrated that the flow dynamics parameters are sensitive to the normalised particle size δ/h. The particle size of the sediment flow principally governs the grain stresses and hence its flow dynamics (Iverson, 1997; McArdell *et al*., 2007; Bowman *et al*., 2010) as described by the Savage number (Savage & Hutter, 1989)

$$N_{sav} = \frac{\dot{\gamma}^2\delta^2}{\boldsymbol{g}h\tan\phi} \tag{1}$$

where δ is the characteristic particle diameter; $\boldsymbol{g}$ is the gravitational acceleration; h is the flow depth; ϕ is the dynamic friction angle of the flow and $\dot{\gamma}$ is the depth-averaged shear rate. To estimate the shear rate $\dot{\gamma}$, the velocity profile along the direction orthogonal to the bed was assumed to be linear. The shear rate is calculated as $\dot{\gamma} = \mathrm{d}v/\mathrm{d}h$ (Kaitna *et al*., 2007; Hsu *et al*., 2014), where v is the velocity at the flow surface and h is the flow height. When $N_{Sav} < 0{\cdot}1$, the grain contact stresses tend to dominate, whereas when $N_{Sav} > 0{\cdot}1$ the inertial grain stresses tend to dominate (Savage & Hutter, 1989).

To intercept geophysical flows, structural countermeasures such as rigid barriers (Lo, 2000) are often installed along the predicted flow path. Flows impacting rigid barriers tend to transfer momentum vertically into run-up, potentially overspilling the barrier (Jiang & Zhao, 2015;

Ng *et al.*, 2016; Choi *et al.*, 2016b). To control overspilling, it is imperative to understand the run-up mechanics holistically and be able to predict maximum run-up heights (Kwan, 2012).

Run-up mechanisms have been investigated using small-scale flume modelling for uniform single-phase flows (Chu *et al.*, 1995; Mancarella & Hungr, 2010; Choi *et al.*, 2015). However, the aforementioned studies adopt monodisperse dry granular or pure water flows for studying the run-up mechanisms, without investigating the influence of particle size itself. Explicit consideration of particle size effect is important as it influences the energy attenuation during impact (Ashwood & Hungr, 2016; Koo *et al.*, 2016; Choi *et al.*, 2016a). Jiang *et al.* (2015) have adopted three types of natural granular materials to study the effects of dynamic internal friction angle and particle diameter on the impact process. Results demonstrate that particle characteristics have profound effects on the impact force. Choi *et al.* (2016a) have investigated the influence of flows with different particle sizes impacting slit structures using glass spheres, demonstrating that large grains resulted in significant saltation, implying that the particle size is an important parameter to consider for flow–structure interaction. Two commonly adopted approaches for predicting run-up have been proposed by Jóhannesson *et al.* (2009) and Kwan (2012). The details are provided in Appendix 1. The former, an energy-based approach, neglecting energy losses is given as follows

$$\frac{h_f}{h} = 1 + \frac{v^2}{2gh} \tag{2}$$

where h_f is the run-up height, h the flow depth, v the flow velocity and g is the acceleration due to gravity. The dimensionless group $v^2/(gh\cos\theta)$ is the Froude number N_{Fr}, indicating the ratio of inertial to gravitational forces. Values of N_{Fr} less than and greater than unity characterise subcritical and supercritical flows, respectively. Another commonly adopted approach proposed by Jóhannesson *et al.* (2009) is based on conservation of mass and momentum and is given as follows

$$\frac{\rho_f}{\rho_i}\left(\frac{h_f}{h_i}\right)^2 - \frac{h_f}{h_i} - 1 + \left(\frac{\rho_f h_f}{\rho_i h_i}\right)^{-1} - 2N_{Fr}^2 = 0 \tag{3}$$

where ρ_f and ρ_i are the density of debris flow in contact with the barrier and upstream flow, respectively. The details are provided in Appendix 1.

In this study, a series of flume experiments were carried out to create dry granular flows to study the effects of particle size on run-up mechanisms, and to investigate the validity of using continuum mechanics in predicting the run-up height on a rigid barrier.

FLUME MODELLING

The 5 m long rectangular flume model (Fig. 1) (Choi *et al.*, 2014) was adopted for this study. The channel has a width and depth of 0·2 and 0·5 m, respectively. The channel is inclinable from 23° to 40° using an overhead crane in the laboratory. The hopper at the top of the flume has a maximum volume of 0·06 m^3.

Scaling

Hübl *et al.* (2009), Zhou & Ng (2010), Armanini (2015) and Iverson (2015) identified the Froude number as a key dimensionless parameter for scaling debris–structure interaction. Also of significance is the ratio between inertial stress and contact stress expressed by N_{sav} (Savage, 1984). To guide the experiment design and to ascertain the governing parameters, a dimensional analysis is provided in Appendix 2.

Instrumentation

The flume model is instrumented with photoconductive sensors (Silonex NORP12 cadmium sulfide), which are installed at regular intervals of 500 mm at the base of the channel. A laser sensor (model: Wenglor YT44MGV) was installed on the top of the flume to measure the flow depth profile just upstream of the barrier. Two high-speed cameras (model: Mikrotron MotionBLITZ EoSens mini2) were used to capture the impact kinematics. The high-speed cameras captured images at 640 frames per second at a resolution of 1400 × 1600. The high-speed camera settings enabled the velocity fields to be interpreted using particle image velocimetry (PIV) (White *et al.*, 2003). Figure 1 shows a side view of the instrumentation set-up.

Test programme

Two types of granular materials were investigated, specifically Leighton Buzzard sand and glass spheres. Fractions E (0·15 mm) and C (0·6 mm) and glass spheres with particle

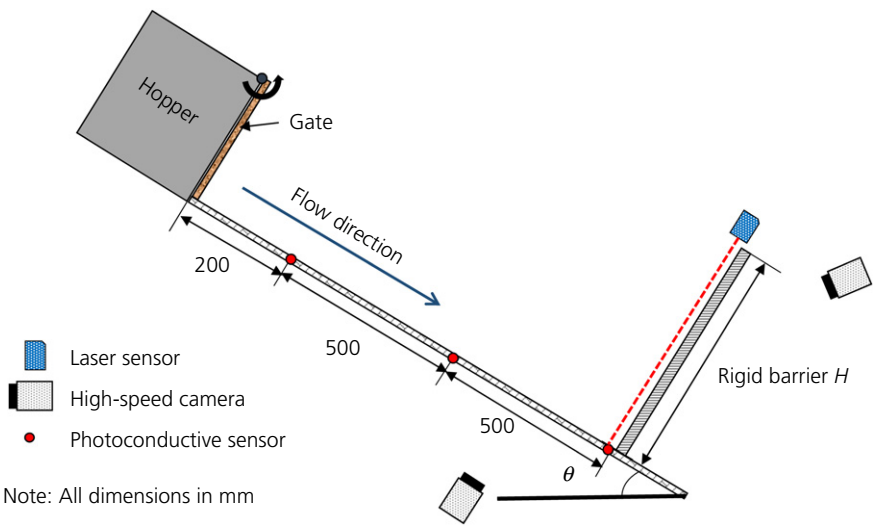

Fig. 1. Side view of the test set-up

Table 1. Material properties

Material type	Leighton Buzzard sand			Glass sphere		
Particle diameter: mm	0·15	0·6	3·0	10·0	23·0	40·0
Dynamic friction angle: deg	20·6	22·6	17·8	16·6	11·6	11·7
Solid density: kg/m^3		2650			2550	
Bulk density: kg/m^3	1700	1680	1620	1611	1583	1513

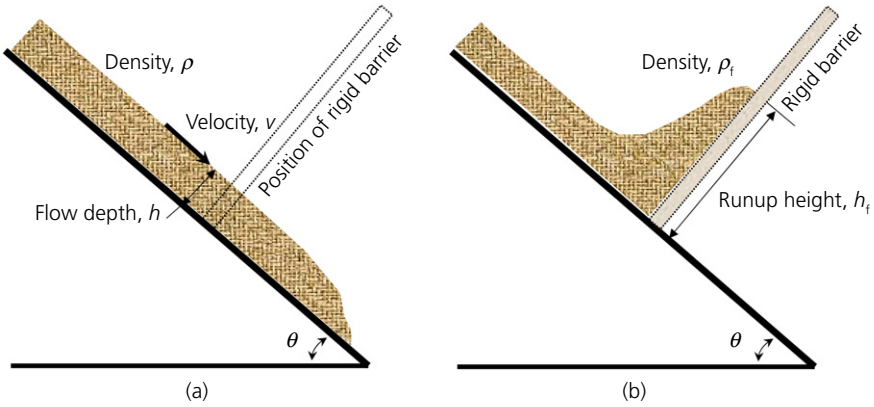

Fig. 2. Side view of the: (a) control test and (b) run-up test

diameters of 3·0, 10·0, 23·0 and 40·0 mm were adopted. The dynamic friction angle of the test material was measured by means of tilting tests referring to Pudasaini & Hutter (2007), Hungr (2008), Mancarella & Hungr (2010). The granular material was deposited on a 0·1 m high straight-faced pile on the channel base. The channel was gradually inclined to tilt the face of the pile at the pace of a fraction of a degree. A light impact was applied onto the channel side at each step. The dynamic friction angle was recorded as the slope angle of face of the pile when a layer of granular material was observed slowly flowing on the pile face following the agitation. Since the dynamic friction angle depends on the properties of the granular material, the dynamic friction angle varies for different granular materials (Podczeck & Mia, 1996; Mair *et al.*, 2002). The tilting tests indicated that larger particle size have lower dynamic friction angles, whereas the smallest particle size shows the highest dynamic friction angle. This is in agreement with Tan & Newton (1990) and Podczeck & Mia (1996). The material properties are summarised in Table 1. The Froude conditions of the flow before impacting the rigid barrier were varied by adjusting the channel inclination. To characterise the Froude condition and N_{Sav} flows, control tests (Fig. 2(a)) without a rigid barrier were performed for each combination of particle size, material type and channel inclination. Likewise, the run-up test was conducted with a rigid barrier installed within the channel to study the run-up mechanism (Fig. 2(b)). Each run-up test was replicated to ascertain the repeatability of the experiments and error bars are provided in the interpretation below. The test programme is summarised in Table 2 and the test results are summarised in Table 3.

Model set-up and testing procedures

A transparent acrylic rigid barrier with a height, width and thickness of 600, 200 and 10 mm, respectively, was installed orthogonally to the channel at a distance of 1200 mm from the gate. Grids (50 mm × 50 mm) were imposed on the barrier for interpretation of high-speed images. The gate was then secured using a magnetic lock and springs attached to the gate were then loaded to the peripheral frame of the flume model. To ensure that all tests are comparable with the analytical solution based on the energy principle (Kwan, 2012), and conservation of mass and momentum (Jóhannesson *et al.*, 2009), all tests were conducted using the same initial potential energy, and thus mass, specifically 30 kg. The differences of initial bulk density are summarised in Table 1. The channel was then inclined to an appropriate inclination angle. The granular materials were released by deactivating the magnetic lock.

INTERPRETATION OF RESULTS

Run-up kinematics

Figures 3 and 4 show the typical run-up kinematics for supercritical dry sand (test R40-LC) and glass sphere flows (test R40-G40) at a channel inclination of 23°, respectively. The captured kinematics from the high-speed camera is shown on the left and its corresponding PIV analysis (White *et al.*, 2003) is shown on the right. The flow direction is from left to right, and the maximum velocities as captured using PIV are shown.

The dry sand forms a thin wedge-like flow front, approaching the barrier at $t = 0$ s with a measured velocity of 1·8 m/s (Fig. 3(a)). The flow front impacts the rigid barrier and deposits at the base of the rigid barrier (Fig. 3(b)). The velocity decreases by about 11% after impact. Subsequent flow material impacts and piles up on top of the existing deposits, forming a dead zone at the base of the barrier at $t = 0·6$ s (Fig. 3(c)). The ramp-like dead zone transfers the momentum of subsequent granular flow upwards. At $t = 0·9$ s (Fig. 3(d)), the maximum velocity of the approaching sand is reduced by 50%, the maximum pileup height is reached, and the impact process rapidly attenuates thereafter. The experimental result of the sand flow predominantly exhibits a pileup mechanism, where the sand layers on top of the deposits at the base of the barrier. The mechanism is in agreement with Armanini *et al.* (2011) and Choi *et al.* (2015).

Table 2. Test programme

Test type	Test ID*	Channel inclination, θ: deg	Flow material	Particle diameter, δ: mm
Control test (without barrier)	C23-LE	23	Leighton Buzzard sand	0·15
	C23-LC			0·60
	C23-G3		Glass sphere	3
	C23-G10			10
	C23-G23			23
	C23-G40			40
	C40-LE	40	Leighton Buzzard sand	0·15
	C40-LC			0·60
	C40-G3		Glass sphere	3
	C40-G10			10
	C40-G23			23
	C40-G40			40
Run-up test (with barrier)	R23-LE	23	Leighton Buzzard sand	0·15
	R23-LC			0·60
	R23-G3		Glass sphere	3
	R23-G10			10
	R23-G23			23
	R23-G40			40
	R40-LE	40	Leighton Buzzard sand	0·15
	R40-LC			0·60
	R40-G3		Glass sphere	3
	R40-G10			10
	R40-G23			23
	R40-G40			40

*C23-G10: C denotes the test type: control test/run-up test, 23 denotes the channel inclination, G denotes the flow material: glass sphere/Leighton Buzzard sand, 10 denotes the particle diameter.

Table 3. Summary of test results

Test ID	Flow velocity, v: m/s high-speed camera	Flow depth, h: m	Particle size to flow depth ratio, δ/h	Shear rate, $\dot{\gamma} = \mathrm{d}v/\mathrm{d}h$	Froude number	Savage number	Normalised run-up height, h_f/h
R23-LE	1·15	0·011	0·01	104·55	3·65	0·006	4·00
R23-LB	1·25	0·012	0·05	104·17	3·80	0·080	4·33
R23-G3	1·75	0·022	0·14	79·55	3·93	0·687	6·55
R23-G10	2·1	0·031	0·32	67·74	3·97	5·062	7·19
R23-G23	2·23	0·035	0·66	63·71	3·97	30·472	7·74
R23-G40	2·63	0·045	0·89	58·44	4·13	59·786	8·11
R40-LE	1·73	0·014	0·01	123·57	5·33	0·007	5·57
R40-LB	1·84	0·015	0·04	122·67	5·48	0·088	5·93
R40-G3	2·24	0·024	0·13	93·33	5·27	0·868	8·38
R40-G10	2·73	0·035	0·29	78·00	5·32	5·944	8·71
R40-G23	2·99	0·042	0·55	71·19	5·32	31·702	9·19
R40-G40	3·55	0·054	0·74	65·74	5·57	63·038	9·85

The flow front comprising glass spheres approaches the rigid barrier at $t = 0$ s with a maximum velocity of 3·6 m/s (Fig. 4(a)). The glass spheres impact the barrier and saltation of grains is observed at the barrier face (Fig. 4(b)). The maximum velocity decreases by about 5%. As the impact process continues, the glass spheres run up along the face of the barrier. Discrete particles reach the maximum run-up height before free-falling back towards the flow mass (Fig. 4(c)). Eventually, the glass spheres rest against the rigid barrier to form a coherent deposition (Fig. 4(d)). The run-up kinematics observed for large glass spheres are more reminiscent of the vertical jet mechanism described by Armanini *et al.* (2011) and Choi *et al.* (2015) for liquid flows.

Tests show that the observed run-up kinematics between dry sand and glass sphere flows are distinct. The dry sand flows have piled up to form the gradually increasing dead zone. On the other hand, the glass sphere flows saltate upon impacting the rigid barrier and the particles discretely run up along the barrier. The relative weighting of contact and inertial flow stresses is responsible for the observed run-up mechanisms. More frictional flows rapidly piled up, forming a pronounced dead zone and shielding the barrier from subsequent materials. By contrast, inertial flows were discrete, exhibited distinct saltation and formed less pronounced dead zone. This observation is consistent with that reported by Bryant *et al.* (2014) in their flume tests where large grain diameters led to greater saltation. Certainly, a more pronounced dead zone is effective in shielding the barrier from the subsequent flow, and transferring the momentum vertically instead of directly into the barrier.

Influence of the bulk Froude conditions on run-up height

Figure 5 shows typical upstream views captured using a high-speed camera installed behind the transparent rigid barrier for glass spheres (tests R40-G23, R40-G10 and R40-G3) and sand (test R40-LC), respectively. The run-up height (h_f) for glass spheres comprise discrete spheres separated from the main flow mass. By contrast, the pileup height for dry sand flow remains coherent during the impact process.

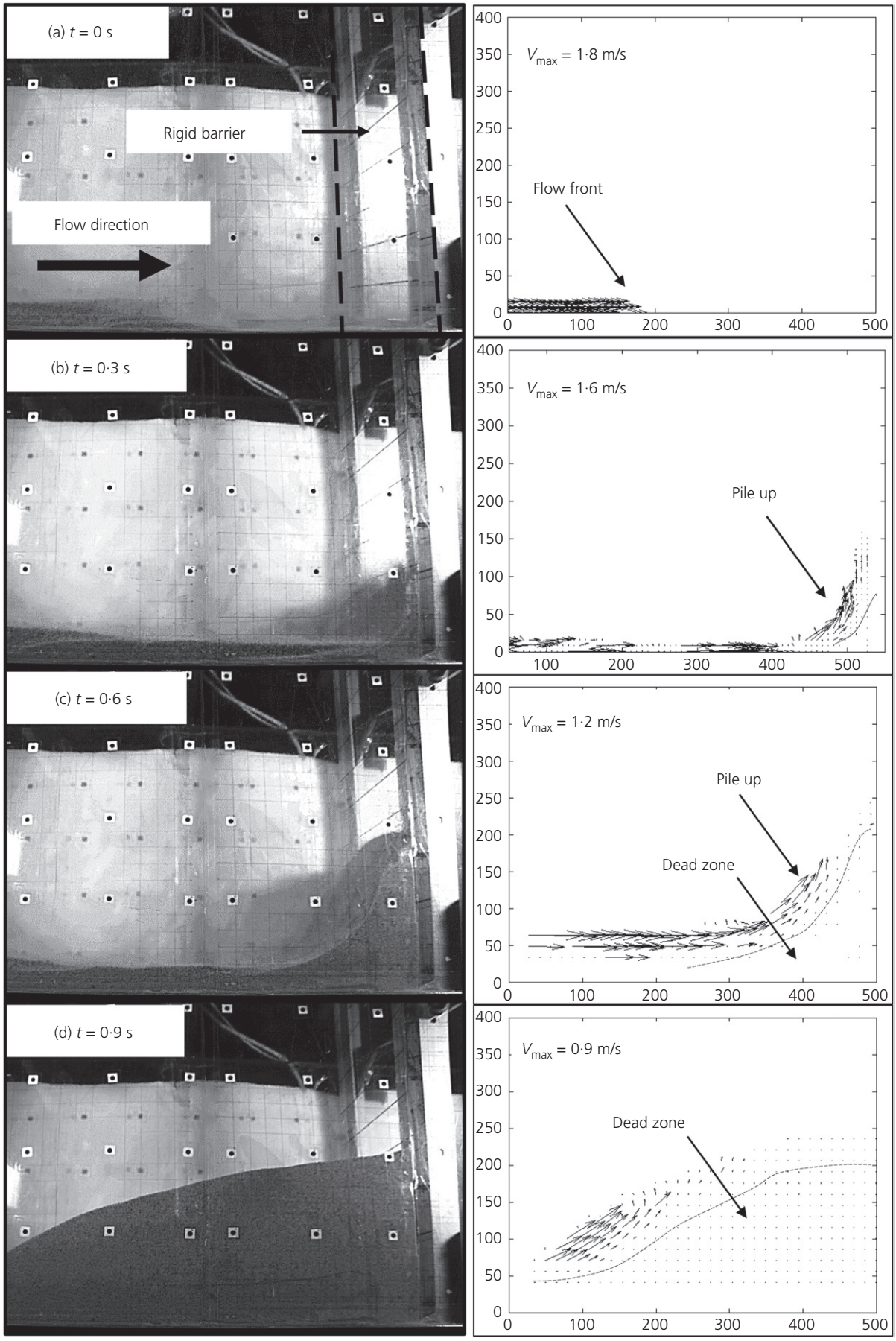

Fig. 3. Observed run-up mechanism for sand flow from side camera and PIV analysis (test R40-LC): (a) $t = 0$ s, (b) $t = 0{\cdot}3$ s, (c) $t = 0{\cdot}6$ s and (d) $t = 0{\cdot}9$ s

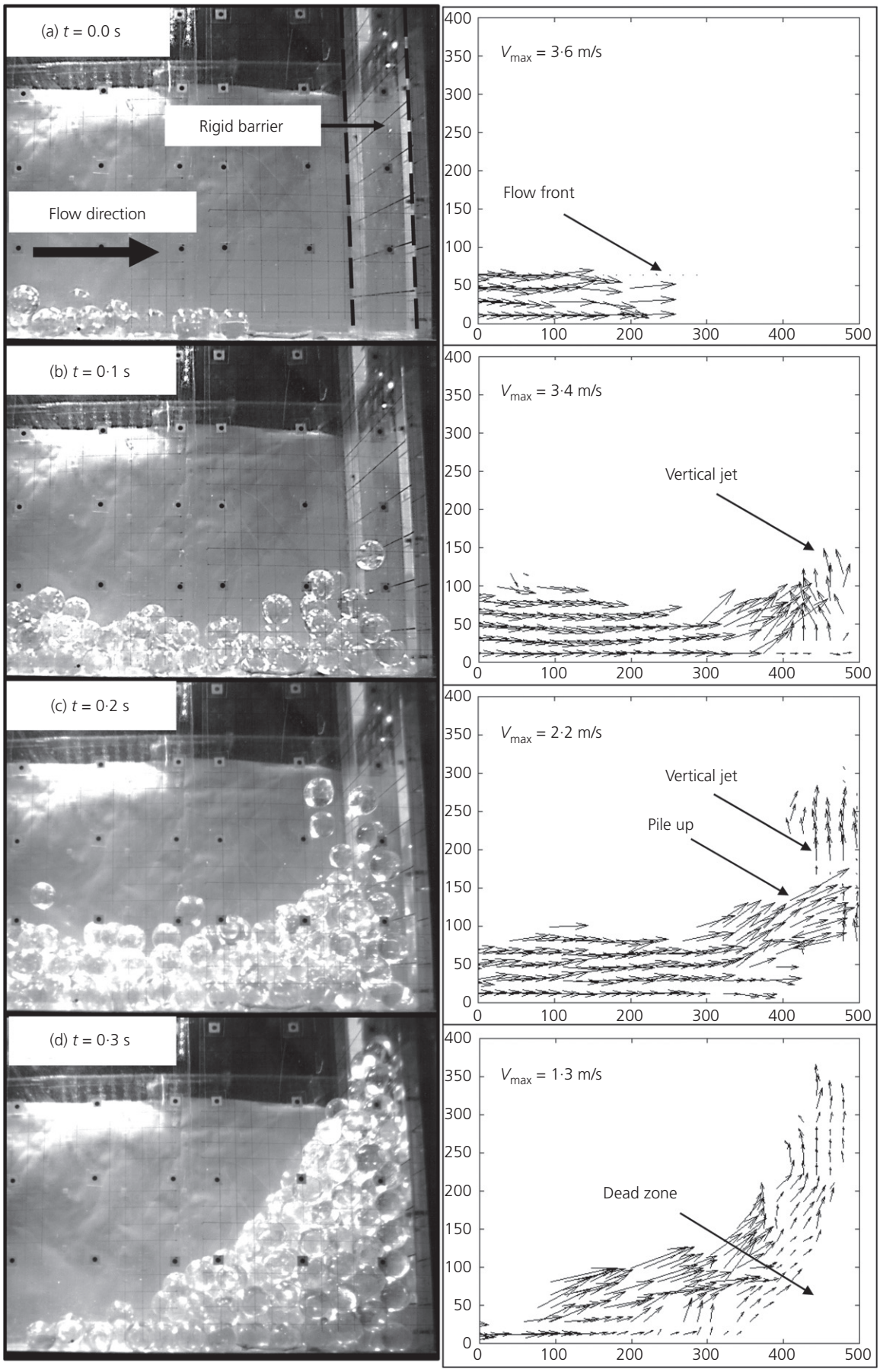

Fig. 4. Observed run-up mechanism for glass sphere flow from side camera and PIV analysis (test R40-G40): (a) $t = 0{\cdot}0$ s, (b) $t = 0{\cdot}1$ s, (c) $t = 0{\cdot}2$ s and (d) $t = 0{\cdot}3$ s

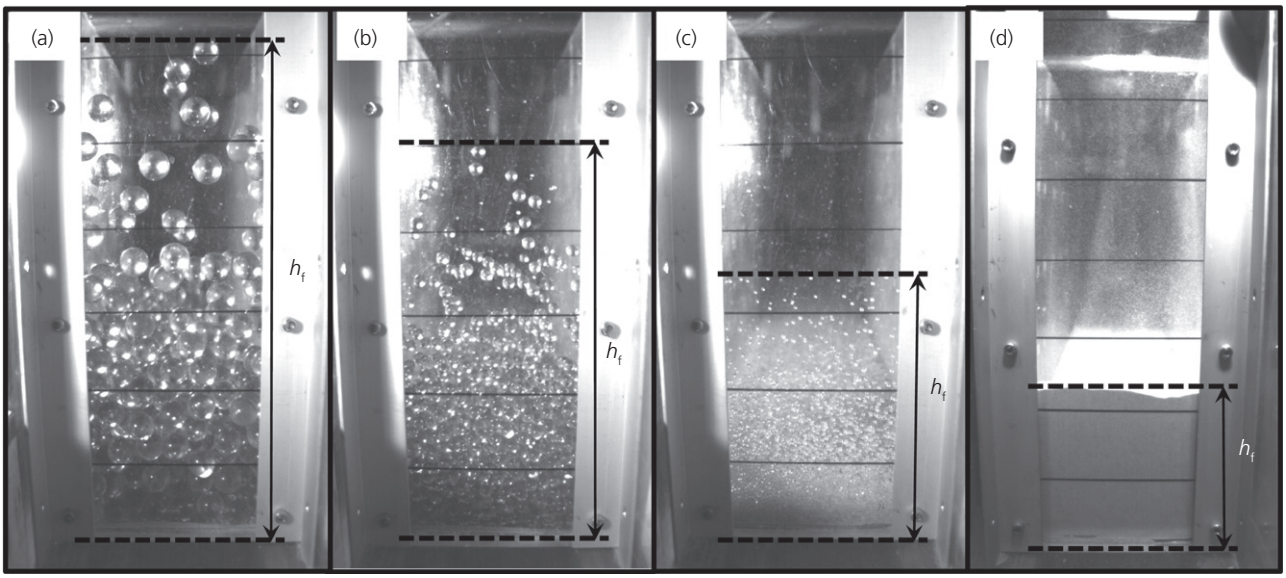

Fig. 5. Upstream view of typical run-up heights: (a) test R40-G23, (b) test R40-G10, (c) test R40-G3 and (d) test R40-LC

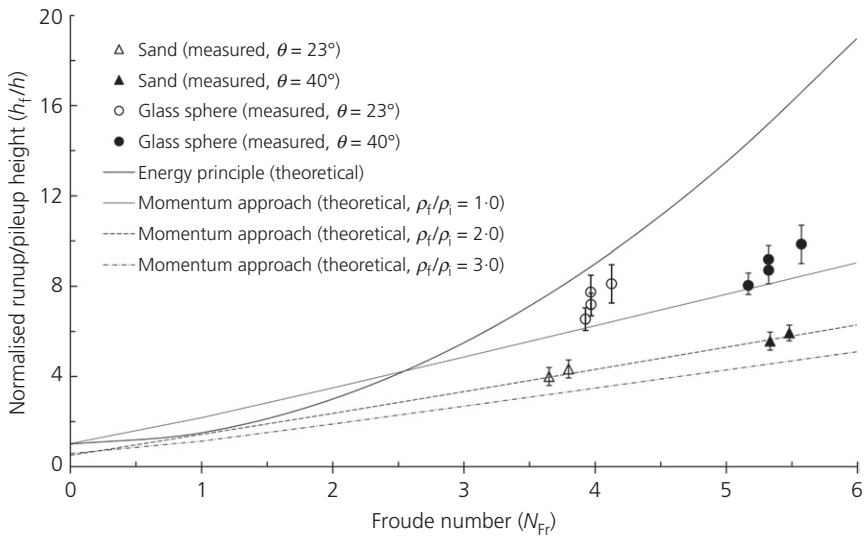

Fig. 6. Comparison of measured normalised run-up height with energy principle (Kwan, 2012) and the momentum approach (Jóhannesson *et al*., 2009)

Figure 6 shows the influence of the upstream Froude conditions (N_{Fr}) before impacting the normalised run-up height (h_f/h) for 30 kg of sand and glass spheres with varying particle diameters (δ) at inclinations of 23° and 40°. Reference lines for the energy principle (Kwan, 2012) and momentum-based approach proposed by Jóhannesson *et al.* (2009) are shown for reference. The energy principle acts as an upper bound since it does not consider the energy loss.

The measured results show that the N_{Fr} of the granular flows generally increases with the channel inclination. This is due to the gravitational component of the flow increases and leads to higher flow velocities and higher shear rates which spread the granular mass along the flow direction (Choi *et al*., 2015), and thus reducing the flow thickness. The energy principle overpredicts the run-up height by up to three times and is not suitable for frictional flows (Choi *et al*., 2015). On the other hand, the momentum-based approach more closely captures the pileup height for dry sand flows. Results indicate that a density ratio (ρ_f/ρ) of 1 can capture the measured pileup heights.

For comparable upstream Froude conditions before impact, glass sphere flows exhibit run-up heights that are almost two times higher than that of dry sand flows. Glass sphere flows have larger particle diameters compared with dry sand flows, which are much more inertial when characterising the flows using the N_{Sav}. The inertial nature of the flows enables the particles to separate from the flow mass during the run-up process.

Influence of particle diameter on run-up height

Figure 7 shows the influence of particle size on flow dynamics described by the Savage number. The Savage number indicates the relative significance of contact and inertial grain stresses in a granular flow. The measured results show that the Savage number increases when the normalised particle size becomes larger. This implies that flows comprising larger particles are more inertial. To highlight the effect of particle size on flow dynamics, when $\delta/h = 1$, a granular flow has a single layer of large particles.

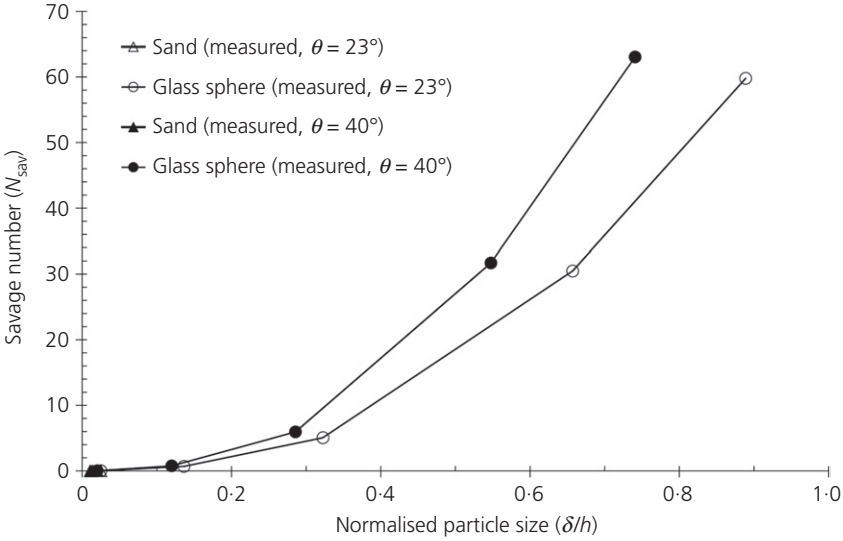

Fig. 7. The effect of normalised particle size on Savage number

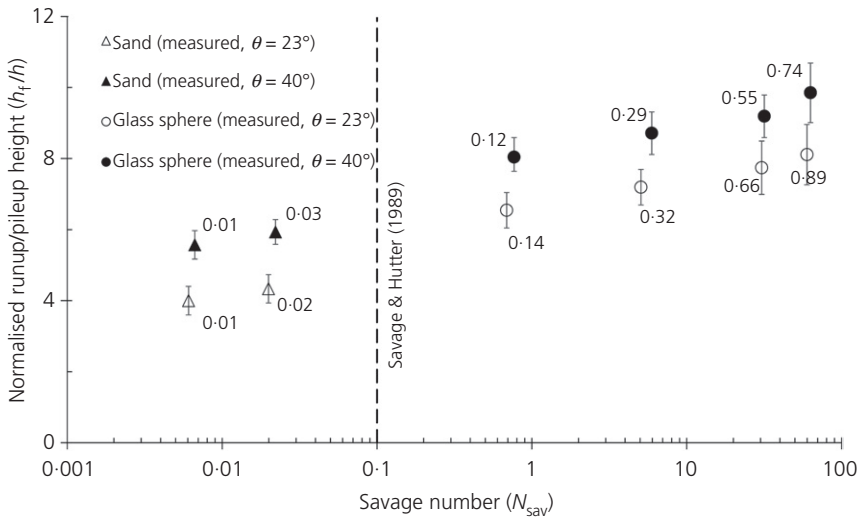

Fig. 8. Influence of Savage number on run-up height (the normalised particle size δ/h for each test is labelled)

Therefore, the Savage number is infinitely large since no contact shearing exists. In this study, δ/h affects the flow dynamics significantly, which is in agreement with the findings of Pouliquen (1999).

Figure 8 shows the influence of grain stresses using the N_{Sav} on the normalised run-up height. The empirical threshold value of $N_{Sav} = 0{\cdot}1$ (Savage & Hutter, 1989), characterising whether a flow is dominated by frictional or inertial stresses, is shown for reference. The measured results show that the glass sphere flows are dominated by inertial stresses ($N_{Sav} > 0{\cdot}1$), whereas dry sand flows in this study are dominated by contact stresses ($N_{Sav} < 0{\cdot}1$). This is because more energy is dissipated through the contact stress (Sovilla *et al.*, 2008). However, for glass sphere flow dominated by inertial stress, less contact stresses exist among the particles. Moreover, the large particles exhibit a discrete nature and demonstrate grain saltation (Groh *et al.*, 2010).

CONCLUSIONS

A series of flume experiments were carried out to study the effects of particle size on dry granular run-up mechanisms. The conclusions drawn are based on the results from a reduced scale flume model. Small-scale modelling cannot capture all fundamental aspects of prototype flows since the geomaterial behaviour is stress-state dependent (Ng *et al.*, 2016). More specifically, under reduced stress conditions, the soil will undergo dilation rather than an expected contractive response under prototype conditions (Iverson & George, 2014). Furthermore, the glass spheres used in this study are perfectly round and have smooth surfaces which are a simplification of the coarse particles in natural geophysical flows. In reality, coarse particles in prototype flows are irregular and rough, which may lead to lower shear rates (Mollon & Zhao, 2013). The simplification made in this study will lead to conservative run-up heights.

- The particle size affects the flow dynamics described by the Savage number significantly. In this study, the Savage number increases when the normalised particle becomes larger since the contact stress surpasses the shearing stress.
- The run-up height is not only dependent on the Froude number of the flow before impact, but also on the particle

size which principally governs the run-up mechanism. Inertial flows comprising large grains ($N_{Sav} > 0{\cdot}1$) profoundly transfers momentum vertically upon impact, resulting in significant saltation and high run-up heights. This implies that large particles accumulating at the flow front can dangerously saltate over a rigid barrier; whereas, frictional flows comprising fine particles ($N_{Sav} < 0{\cdot}1$) tend to pile up due to a high degree of contact stresses, resulting in a coherent impact process without significant run-up. Results indicate that both Froude and Savage numbers should be considered in a run-up assessment.

- The momentum approach based on continuum mechanics underestimates the run-up height of granular flows comprising large particles. This indicates that for landslides such as rock avalanches and boulder-entrained debris flow, the particle size must be taken into account to consider the discrete nature of the run-up process and to ensure a conservative prediction of run-up height.

The series of flume experiments is aimed at investigating the effect of particle size and run-up mechanism. By varying the particle size of the granular material for each test, the dynamic friction angle also changed correspondingly. The effect of the dynamic friction angle is reflected in the Savage number ($N_{sav} = \gamma^2\delta^2/\boldsymbol{g}h\tan\phi$). The larger particle size leads to a smaller dynamic friction angle, and thus a larger Savage number, which is inversely proportional to the dynamic friction angle.

ACKNOWLEDGEMENTS

The authors acknowledge the financial support from research grant T22-603/15-N provided by the Research Grants Council of the Government of Hong Kong SAR, China, and the HKUST Jockey Club Institute for Advanced Study for their support.

APPENDIX 1: EQUATIONS OF RUN-UP

A1.1 Energy principle

The debris run-up height against a vertical rigid barrier can be calculated using the energy principle (Armanini *et al.*, 2011; Kwan, 2012). The flow is assumed as a homogeneous material that retains its macroscopic shape as it travels with speed v and thickness h on a uniform and frictionless slope in vacuum. No energy losses occur during the impact process. The conservation of energy is expressed as follows

$$E_i = E_f \tag{4}$$

where E_i is the initial energy of the flow approaching the rigid barrier and E_f is the final energy of the flow impacting the rigid barrier.

The initial energy of debris flows approaching the rigid barrier is shown as follows

$$E_i = \frac{1}{2}mv^2 + m\boldsymbol{g}h \tag{5}$$

where m is the mass of the flow, $\boldsymbol{g}$ the gravitational acceleration and h is the flow depth.

The final energy of debris flows impacting the rigid barrier at its maximum height

$$E_f = m\boldsymbol{g}h_f \tag{6}$$

where h_f is the run-up height of flow impacting the rigid barrier.

Substituting equations (5) and (6) into equation (4)

$$\frac{1}{2}mv^2 + m\boldsymbol{g}h = m\boldsymbol{g}h_f \tag{7}$$

The run-up height on the rigid barrier is therefore

$$h_f = h + \frac{v^2}{2\boldsymbol{g}} \tag{8}$$

The normalised run-up height by flow depth h can be expressed as

$$\frac{h_f}{h} = 1 + \frac{v^2}{2\boldsymbol{g}h} \tag{9}$$

A1.2 Momentum approach

Jóhannesson *et al.* (2009) have proposed an analytical solution for the calculation of the run-up height of an avalanche against a rigid barrier in a uniform channel. The equation is derived based on the conservation of mass and momentum for a shock that occurs during the impact process of a shallow flow (see also Hákonardóttir *et al.*, 2003; Zanuttigh & Lamberti, 2006). As shown in Fig. 9, a jump forms as the flow impacts the rigid barrier. Subsequently, a bore propagates upstream of the rigid barrier with speed u. By choosing a reference frame travelling with the bore at speed u upstream, the run-up height based on the conservation of mass is expressed as follows

$$(v + u)h\rho_i = uh_f\rho_f \tag{10}$$

where ρ_i is the density of the approaching flow and ρ_f is the density of the flow impacting the rigid barrier.

The conservation of momentum is expressed by

$$h\rho_i(v + u)^2 + \frac{1}{2}\boldsymbol{g}\rho_i h^2 = h_f\rho_f u^2 + \frac{1}{2}\boldsymbol{g}\rho_f h_f^2 \tag{11}$$

The reference frame travels with the granular bore. Its velocity u can be expressed as

$$u = \frac{vh\rho_i}{(h_f\rho_f - h\rho_i)} \tag{12}$$

Substituting equation (11) into equation (10), the momentum conservation can be expressed as

$$\frac{\rho_f}{\rho_i}\left(\frac{h_f}{h_i}\right)^2 - \frac{h_f}{h_i} - 1 + \left(\frac{\rho_f h_f}{\rho_i h_i}\right)^{-1} - 2\frac{v^2}{\boldsymbol{g}h} = 0 \tag{13}$$

The expression, relating the run-up height, the depth of the approaching flow, density ratio and the Froude number,

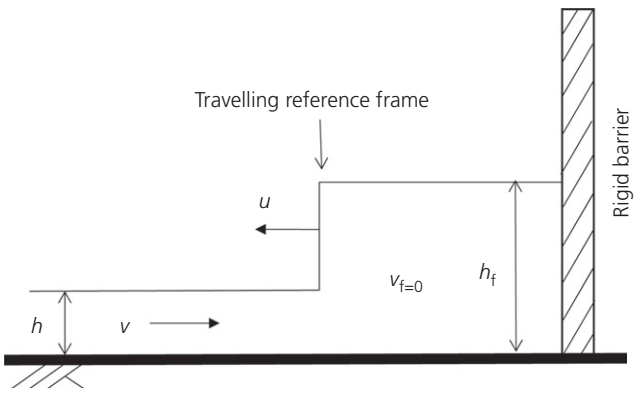

Fig. 9. Schematic drawing of a two-dimensional bore travelling upstream of the rigid barrier at speed u

is given by

$$\frac{\rho_f}{\rho_i}\left(\frac{h_f}{h_i}\right)^2 - \frac{h_f}{h_i} - 1 + \left(\frac{\rho_f h_f}{\rho_i h_i}\right)^{-1} - 2N_{Fr}^2 = 0 \tag{14}$$

APPENDIX 2: DIMENSIONAL ANALYSIS OF DRY GRANULAR FLOW

A dimensional analysis (Savage, 1984; Iverson, 2015) by using Buckingham Π group was carried out to guide the experimental set-up and ascertain the governing dimensionless group. The Froude number and Savage numbers are identified as the two key parameters governing the flow in an inclined channel.

A2.1 MACROSCOPIC ANALYSIS

The dimensional analysis conducted by Iverson (2015) assumes a block with homogeneous material travelling down an inclined plane in vacuum. The speed v can be expressed using the following variables

$$v = f_1(\boldsymbol{g}, L, h, \rho, \theta, \sigma, \phi, t) \tag{15}$$

where $\boldsymbol{g}$ is the gravitational acceleration; L is the length of the block; h is the flow depth; ρ is the bulk density; θ is the channel inclination; σ is a generic stress variable, describing the effects of internal deformation on energy dissipation; ϕ is the dynamic friction angle; and t is the travel time.

θ and ϕ are intrinsically dimensionless and play no role in the identification of dimensionless variables. Buckingham's Π theorem indicates that the other seven dimensional variables must be related and can be expressed using four independent dimensionless variables. To ascertain the four variables, the function equation (15) is postulated to have the generic relationship

$$v = k\boldsymbol{g}^a L^b h^c \rho^d \sigma^e t^f \tag{16}$$

By expressing all physical variables in equation (16) by mass $[M]$, length $[L]$ and time $[T]$

$$\frac{[L]}{[T]} = \left(\frac{[L]}{[T]^2}\right)^a [L]^b [L]^c \left(\frac{[M]}{[L]^3}\right)^d \left(\frac{[M]}{[L][T]^2}\right)^e [T]^f$$

To achieve the dimensional homogeneity, three conditions must be satisfied

$$[M] : 0 = d + e$$

$$[L] : 1 = a + b + c - 3d - e$$

$$[T] : -1 = -2a - 2e + f$$

Therefore, the unknowns a, b, d can be algebraically eliminated by substituting c, e, f

$$v = k(\boldsymbol{g}L)^{1/2}\left(\frac{h}{L}\right)^c \left(\frac{\sigma}{\rho \boldsymbol{g} L}\right)^e \left(\frac{t}{(L/\boldsymbol{g})^{1/2}}\right)^f \tag{17}$$

Equation (17) can be rewritten in dimensionless form as

$$\frac{v}{(\boldsymbol{g}L)^{1/2}} = f_2\left(\frac{h}{L}, \frac{\sigma}{\rho \boldsymbol{g} L}, \frac{t}{(L/\boldsymbol{g})^{1/2}}, \theta, \phi\right) \tag{18}$$

where $v/(\boldsymbol{g}L)^{1/2}$ is the Froude number (the ratio of the inertial force to the gravitational force); h/L is the length scale; $\sigma/\rho \boldsymbol{g} L$ is the scaled stress; and $t/(L/\boldsymbol{g})^{1/2}$ is the time scale for motion.

A2.2 MICROSCOPIC ANALYSIS

The dimensional analyses of steady, uniform shear flows build on the foundation established by Savage's (1984) analysis of dry granular flows. Correspondingly, the deviatoric stress $\bar{\boldsymbol{\tau}}_{ij}$ can be expressed as

$$\bar{\boldsymbol{\tau}}_{ij} = \boldsymbol{\tau}_{ij} - \frac{1}{3}\tau_{kk}\boldsymbol{\sigma}_{ij} = \boldsymbol{\tau}_{ij} - p\boldsymbol{\sigma}_{ij} \tag{19}$$

where $\boldsymbol{\tau}_{ij}$ is the stress tensor and, p is the mean normal stress.

The deviatoric stress $\bar{\boldsymbol{\tau}}_{ij}$ and pressure p can be expressed as

$$\bar{\boldsymbol{\tau}}_{ij} = f_3\left(\rho_P,\ \dot{\gamma}, \langle v^2\rangle^{1/2}, \langle w^2\rangle^{1/2}, p, \upsilon, \delta, h, \boldsymbol{g}, e, \mu, E, s\right) \tag{20}$$

$$p = f_3\left(\rho_P, \dot{\gamma}, \langle v^2\rangle^{1/2}, \langle w^2\rangle^{1/2}, \upsilon, \delta, h, P_B, \boldsymbol{g}, e, \mu, E, s\right) \tag{21}$$

where ρ_P is the solid density of the granular material; $\dot{\gamma}$ is the shear rate; $\langle v^2\rangle^{1/2}$ and $\langle w^2\rangle^{1/2}$ are the translational and rotational velocity from particle interaction; υ is the solids fraction; δ is the particle diameter; h is the depth shear flow; $\boldsymbol{g}$ is the gravitational acceleration; P_B is the normal stress applied at the boundary of the shear region; e, μ and E are the coefficient of restitution, the surface coefficient of friction and the modulus of elasticity of the solid particles, respectively; and s is a factor describing the angularity or sphericity of the solid particles.

Dimensional homogeneity requires

$$\frac{\bar{\boldsymbol{\tau}}_{ij}}{\rho_p \delta^2 \dot{\gamma}^2} = f_4\left(\frac{P}{\rho_p \delta^2 \dot{\gamma}^2}, \frac{\delta\dot{\gamma}}{\langle v^2\rangle^{1/2}}, \frac{\dot{\gamma}}{\langle w^2\rangle^{1/2}}, \frac{\boldsymbol{g}}{\delta\dot{\gamma}^2}, \upsilon, \frac{\delta}{h}, \frac{P}{E}, e, \mu, s\right) \tag{22}$$

$$\frac{P}{\rho_p \delta^2 \dot{\gamma}^2} = f_4\left(\frac{\delta\dot{\gamma}}{\langle v^2\rangle^{1/2}}, \frac{\dot{\gamma}}{\langle w^2\rangle^{1/2}}, \frac{\boldsymbol{g}}{\delta\dot{\gamma}^2}, \frac{\rho_p \delta^2 \dot{\gamma}^2}{P_B}, \frac{P_B}{E}, \upsilon, \frac{\delta}{h}, \frac{P}{E}, e, \mu, s\right) \tag{23}$$

For fluid-like flow regime, if the shear rates and stress level are high enough, so that the gravity effect is insignificant, then the dimensionless group $\boldsymbol{g}/\delta\dot{\gamma}^2$ tends to 0. If the shear rates and stress level are low enough, so that the particles can be regarded as rigid, then the dimensionless group P/E tends to 0. $\delta\dot{\gamma}/\langle v^2\rangle^{1/2}$ and $\dot{\gamma}/\langle w^2\rangle^{1/2}$ are the normalised translational and rotational velocity from particle interaction; δ/h is the normalised particle diameter. The dimensionless group $\rho_p \delta^2 \dot{\gamma}^2 / P_B$, which is proportional to the ratio of the dynamic or collisional stresses to total boundary stress, is the primary parameter that distinguishes the various flow regimes for dry granules. It can be rewritten as

$$N_{sav} = \frac{\rho_p \delta^2 \dot{\gamma}^2}{P_B} = \frac{\rho_p \dot{\gamma}^2 \delta^2}{\rho_p \boldsymbol{g} h \tan\phi} = \frac{\dot{\gamma}^2 \delta^2}{\boldsymbol{g} h \tan\phi} \tag{24}$$

REFERENCES

Armanini, A. (2015). Closure relations for mobile bed debris flows in a wide range of slopes and concentrations. *Adv. Water Resour.* **81**, No. 7, 75–83.

Armanini, A., Larcher, M. & Odorizzi, M. (2011). Dynamic impact of a debris flow front against a vertical wall. In *5th international conference on debris-flow hazards. Mitigation, mechanics, prediction and assessment*, Padua, Italy (eds R. Genevois, D. L. Hamilton and A. Prestininzi),

pp. 1041–1049. Rome, Italy: Casa Editrice Università La Sapienza.

Ashwood, W. & Hungr, O. (2016). Estimating total resisting force in flexible barrier impacted by a granular avalanche using physical and numerical modelling. *Can. Geotech. J.* **53**, No. 10, 1700–1717.

Bowman, E. T., Laue, J., Imre, B. & Springman, S. M. (2010). Experimental modelling of debris flow behaviour using a geotechnical centrifuge. *Can. Geotech. J.* **47**, No. 7, 742–762.

Bryant, S. K., Take, W. A. & Bowman, E. T. (2014). Observations of grain-scale interactions and simulation of dry granular flows in a large-scale flume. *Can. Geotech. J.* **52**, No. 5, 638–655.

Choi, C. E., Ng, C. W. W., Song, D., Kwan, J. S. H., Shiu, H. Y. K., Ho, K. K. S. & Koo, R. C. H. (2014). Flume investigation of landslide debris baffles. *Can. Geotech. J.* **51**, No. 5, 540–533.

Choi, C. E., Au-Yeung, S. C. H. & Ng, C. W. W. (2015). Flume investigation of landslide granular debris and water runup mechanisms. *Géotech. Lett.* **5**, No. 1, 28–32, http://dx.doi.org/10.1680/geolett.14.00080.

Choi, C. E., Goodwin, G., Ng, C. W. W., Chu, H. K., Kwan, J. S. H. & Pun, W. K. (2016a). Coarse granular flow interaction with slit-structures. *Géotech. Lett.* **6**, No. 4, 267–274, http://dx.doi.org/10.1680/jgele.16.00103.

Choi, C. E., Ng, C. W. W., Goodwin, G. R., Liu, L. H. D. & Cheung, W. W. (2016b). Flume investigation of the influence of rigid barrier deflector angle on dry granular overflow mechanisms. *Can. Geotech. J.* **53**, No. 10, 1751–1759.

Chu, T., Hill, G., McClung, D. M., Ngun, R. & Sherkat, R. (1995). Experiments on granular flows to predict avalanche runup. *Can. Geotech. J.* **32**, No. 2, 285–295.

Gray, J. M. N. T. & Chugunov, V. A. (2006). Particle-size segregation and diffusive remixing in shallow granular avalanches. *J. Fluid Mech.* **569**, 365–398.

Groh, C., Rehberg, I. & Kruelle, C. A. (2010). Particle dynamics of a cartoon dune. *New J. Phys.* **12**, No. 6, 063025.

Hákonardóttir, K. M., Hogg, A. J., Jóhannesson, T. & Tómasson, G. G. (2003). A laboratory study of the retarding effects of braking mounds on snow avalanches. *J. Glaciology* **49**, No. 165, 191–200.

Hsu, L., Dietrich, W. E. & Sklar, L. S. (2014). Mean and fluctuating basal forces generated by granular flows: laboratory observations in a large vertically rotating drum. *J. Geophys. Res., Earth Surf.* **119**, No. 6, 1283–1309.

Hübl, J., Suda, J., Proske, D., Kaitna, R. & Scheidl, C. (2009). Debris flow impact estimation. In *11th international symposium on water management and hydraulic engineering*, Ohrid, Macedonia, vol. 1, pp. 137–148.

Hungr, O. (2008). Simplified models of spreading flow of dry granular material. *Can. Geotech. J.* **45**, No. 8, 1156–1168.

Iverson, R. M. (1997). The physics of debris flows. *Rev. Geophys.* **35**, No. 3, 245–296.

Iverson, R. M. (2015). Scaling and design of landslide and debris-flow experiments. *Geomorphology* **244**, No. 9, 9–20.

Iverson, R. M. & George, D. L. (2014). A depth-averaged debris-flow model that includes the effects of evolving dilatancy. I. Physical basis. *Proceedings of the Royal Society* **470**, No. 2170, 20130819.

Jakob, M., Hungr, O. & Jakob, D. M. (2005). *Debris-flow hazards and related phenomena*. Berlin, Germany: Springer.

Jiang, Y. J. & Zhao, Y. (2015). Experimental investigation of dry granular flow impact via both normal and tangential force measurements. *Géotech. Lett.* **5**, No. 1, 33–38, http://dx.doi.org/10.1680/geolett.15.00003.

Jiang, Y. J., Zhao, Y., Towhata, I. & Liu, D. X. (2015). Influence of particle characteristics on impact event of dry granular flow. *Powder Technol.* **271**, No. A, 53–67.

Jóhannesson, T., Gauer, P., Issler, P., Lied, K. & Hákonardóttir, K. M. (2009). *The design of avalanche protection dams: recent practical and theoretical developments*, Project report EUR 23339. Brussels, Belgium: European Commission.

Johnson, C. G., Kokelaar, B. P., Iverson, R., Logan, M., LaHusen, R. G. & Gray, J. M. N. T. (2012). Grain-size segregation and levee formation in geophysical mass flows. *J. Geophys. Res., Earth Surf.* **117**, No. F01032, 1–23.

Kaitna, R., Rickenmann, D. & Schatzmann, M. (2007). Experimental study on rheologic behaviour of debris flow material. *Acta Geotech.* **2**, No. 2, 71–85.

Koo, R. C. H., Kwan, J. S. H., Ng, C. W. W., Lam, C., Choi, C. E. & Song, D. (2016). Velocity attenuation of debris flows and a new momentum-based load model for rigid barriers. *Landslides* **1**, No. 5, 1–13.

Kwan, J. S. H. (2012). *Supplementary technical guidance on design of rigid debris-resisting barriers*, Report no. 270. Kowloon, Hong Kong: Geotechnical Engineering Office.

Lo, D. O. K. (2000). *Review of natural terrain landslide debris-resisting barrier design*, Report no. 104. Kowloon, Hong Kong: Geotechnical Engineering Office.

Mair, K., Frye, K. M. & Marone, C. (2002). Influence of grain characteristics on the friction of granular shear zones. *J. Geophys. Res., Solid Earth* **107**, No. B102219, 1–9.

Mancarella, D. & Hungr, O. (2010). Analysis of run-up of granular avalanches against steep, adverse slopes and protective barriers. *Can. Geotech. J.* **47**, No. 8, 827–841.

McArdell, B. W., Bartelt, P. & Kowalski, J. (2007). Field observations of basal forces and fluid pore pressure in a debris flow. *Geophys. Res. Lett.* **34**, No. L07406, 1–4.

Mollon, G. & Zhao, J. (2013). The influence of particle shape on granular Hopper flow. *AIP Conf. Proc.* **1542**, No. 1, 690–693.

Ng, C. W. W., Song, D., Choi, C. E., Kwan, J. S. H., Shiu, H. Y. K. & Koo, R. C. H. (2016). Centrifuge modelling of dry granular and viscous impact on rigid and flexible barriers. *Can. Geotech. J.* **54**, No. 2, 188–206.

Podczeck, F. & Mia, Y. (1996). The influence of particle size and shape on the angle of internal friction and the flow factor of unlubricated and lubricated powders. *Int. J. Pharm.* **144**, No. 2, 187–194.

Pouliquen, O. (1999). Scaling laws in granular flows down rough inclined planes. *Phys. Fluids (1994-present)* **11**, No. 3, 542–548.

Pudasaini, S. P. & Hutter, K. (2007). *Avalanche dynamics: dynamics of rapid flows of dense granular avalanches*. Berlin, Germany: Springer.

Savage, S. B. (1984). The mechanics of rapid granular flows. *Adv. Appl. Mech.* **24**, 289–366.

Savage, S. B. & Hutter, K. (1989). The motion of a finite mass of granular material down a rough incline. *J. Fluid Mech.* **199**, No. 2, 177–215.

Sovilla, B., Schaer, M., Kern, M. & Bartelt, P. (2008). Impact pressures and flow regimes in dense snow avalanches observed at the Vallée de la Sionne test site. *J. Geophys. Res.* **113**, No. F01010, 1–14.

Tan, S. B. & Newton, J. M. (1990). Powder flowability as an indication of capsule filling performance. *Int. J. Pharm.* **61**, No. 1–2, 145–155.

White, D. J., Take, W. A. & Bolton, M. D. (2003). Soil deformation measurement using particle image velocimetry (PIV) and photogrammetry. *Géotechnique* **53**, No. 7, 619–632, http://dx.doi.org/10.1680/geot.2003.53.7.619.

Zanuttigh, B. & Lamberti, A. (2006). Experimental analysis of the impact of dry avalanches on structures and implication for debris flows. *J. Hydraul. Res.* **47**, No. 4, 381–383.

Zhou, G. G. D. & Ng, C. W. W. (2010). Dimensional analysis of natural debris flows. *Can. Geotech. J.* **47**, No. 7, 719–729.

HOW CAN YOU CONTRIBUTE?

To discuss this paper, please submit up to 500 words to the editor at journals@ice.org.uk. Your contribution will be forwarded to the author(s) for a reply and, if considered appropriate by the editorial board, it will be published as a discussion in a future issue of the journal.